

Retraction

Retracted: Deep Learning-Based Identification of Spinal Metastasis in Lung Cancer Using Spectral CT Images

Scientific Programming

Received 3 October 2023; Accepted 3 October 2023; Published 4 October 2023

Copyright © 2023 Scientific Programming. This is an open access article distributed under the Creative Commons Attribution License, which permits unrestricted use, distribution, and reproduction in any medium, provided the original work is properly cited.

This article has been retracted by Hindawi following an investigation undertaken by the publisher [1]. This investigation has uncovered evidence of one or more of the following indicators of systematic manipulation of the publication process:

- (1) Discrepancies in scope
- (2) Discrepancies in the description of the research reported
- (3) Discrepancies between the availability of data and the research described
- (4) Inappropriate citations
- (5) Incoherent, meaningless and/or irrelevant content included in the article
- (6) Peer-review manipulation

The presence of these indicators undermines our confidence in the integrity of the article's content and we cannot, therefore, vouch for its reliability. Please note that this notice is intended solely to alert readers that the content of this article is unreliable. We have not investigated whether authors were aware of or involved in the systematic manipulation of the publication process.

Wiley and Hindawi regrets that the usual quality checks did not identify these issues before publication and have since put additional measures in place to safeguard research integrity.

We wish to credit our own Research Integrity and Research Publishing teams and anonymous and named external researchers and research integrity experts for contributing to this investigation.

The corresponding author, as the representative of all authors, has been given the opportunity to register their agreement or disagreement to this retraction. We have kept a record of any response received.

References

- [1] X. Fan, X. Zhang, Z. Zhang, and Y. Jiang, "Deep Learning-Based Identification of Spinal Metastasis in Lung Cancer Using Spectral CT Images," *Scientific Programming*, vol. 2021, Article ID 2779390, 7 pages, 2021.

Research Article

Deep Learning-Based Identification of Spinal Metastasis in Lung Cancer Using Spectral CT Images

Xiaojie Fan ¹, Xiaoyu Zhang ¹, Zibo Zhang ¹ and Yifang Jiang ²

¹Department of Orthopedics, Fourth Hospital of Hebei Medical University, Shijiazhuang 050011, Hebei, China

²Department of Respiratory, Fourth Hospital of Hebei Medical University, Shijiazhuang 050011, Hebei, China

Correspondence should be addressed to Yifang Jiang; yifangjiang@ecupl.edu.cn

Received 13 May 2021; Revised 8 June 2021; Accepted 18 June 2021; Published 28 June 2021

Academic Editor: Gustavo Ramirez

Copyright © 2021 Xiaojie Fan et al. This is an open access article distributed under the Creative Commons Attribution License, which permits unrestricted use, distribution, and reproduction in any medium, provided the original work is properly cited.

In this study, deep learning algorithm-based energy/spectral computed tomography (CT) for the spinal metastasis from lung cancer was used. A dilated convolutional U-Net model (DC-U-Net model) was first proposed, which was used to segment the energy/spectral CT image of patients with the spinal metastasis from lung cancer. Subsequently, energy/spectral CT images under different energy levels were collected for the signal-to-noise ratio (SNR) and contrast-to-noise ratio (CNR) comparison. It was found the learning rate of the model decreased exponentially as the number of training increased, with the lung contour segmented out of the image. Under 40–65 keV, the CT value of bone metastasis from lung cancer decreased with increasing energy, as with the average rank sum test result. The SNR and CNR values were the highest under 60 keV. The detection rate of the deep learning algorithm below 60 keV was 81.41%, and that of professional doctors was 77.56%. The detection rate of the deep learning algorithm below 140 keV was 66.03%, and that of professional doctors was 64.74%. In conclusion, the DC-U-Net model demonstrates better segmentation effects versus the convolutional neural network (CNN), with the lung contour segmented. Further, a higher energy level leads to worse segmentation effects on the energy/spectral CT image.

1. Introduction

Bone metastasis from lung cancer refers to the transfer of lung cancer cells to the bone tissue through the blood, causing secondary bone damage, which is an important sign of lung cancer entering the advanced stage [1]. Bone diseases caused by lung cancer are mostly osteolytic diseases, with a reported incidence between 10 and 15% [2]. The spine is subjected to a variety of cancer metastases. Lung cancer can invade the thoracic spine backwards or the neck-thoracic junction upwards, or tumor cells in the cerebrospinal fluid shed to form spinal metastases or spinal cord metastases, manifested as back pain and neurological dysfunction clinically [3]. Energy/spectral CT is a major discovery after spiral CT and multislice CT, characteristic of multiparameter imaging such as the base material image, the monoenergetic CT image, and the energy spectrum curve, commonly used for metal artifact and hardening artifact removal, small lesion detection, fine structure display, and vascular imaging [4–6]. Deep learning is a branch

of machine learning based on artificial neural networks, which is dedicated to making machines have the ability to analyze and learn like humans and recognize data such as text, images, and sounds [7]. Recurrent neural network (RNN) has memory, parameter sharing, and Turing completeness, and it demonstrates superb capabilities in learning nonlinear characteristics of sequences. The combination of RNN and convolutional neural network (CNN) can extract image features frame by frame, thereby saving manpower and improving accuracy [8]. DC is used to solve the problem in image segmentation. General image segmentation algorithms mostly use the pooling layer and the convolutional layer to zoom in the receptive field and zoom out the feature map and then restore the image through upsampling. The image will be damaged during the process of zooming in and zooming out, while the DC avoids image loss by replacing the upsampling and downsampling processes [9]. The study aims to improve the diagnostic efficiency of energy/spectral CT images for spinal metastasis from lung cancer.

In this study, the three-dimensional CNN-based DC-U-Net model was used to process CT images of different energy levels. The accuracy of the proposed algorithm was verified factoring into the signal-to-noise ratio and contrast. The image segmentation effects were compared between professional doctors and the proposed model, factoring into the detection rate. The study was expected to provide reference for the clinical diagnosis of bone metastases from lung cancer.

2. Materials and Methods

2.1. The Clinical Data. The imaging data of 36 patients with lung cancer combined with osteolytic spine metastases, undergoing energy/spectral CT scans from October 2018 to June 2020 in hospital, were collected. Inclusion criteria: energy/spectral CT images presented visible osteolytic bone foci in the vertebral body; patients with myeloma diagnosed by bone marrow biopsy; patients with lung cancer bone metastases diagnosed as primary foci; and patients aged 25–65 years, 20 male and 16 female cases. Exclusion criteria: patients who had received antitumor therapy and drugs that affected bone metabolism before energy/spectrum CT examination; patients with severe heart disease and liver and kidney dysfunction.

2.2. The Structure of the Deep Learning Model. The neuron is the basic structure and functional unit of neural structure. The working process of the neuron is shown in Figure 1. Multiple neurons are combined to form a neural network. The neural network is generally multilayered, including the input layer, the hidden layer, and the output layer. The AlexNet model, a classical convolutional neural network, is an eight-layer structure composed of 650,000 neurons, with as many as 60 million parameters. When a 256×256 image is input, more than 1,000 different types are output. The three fully-connected layers have good image processing effects. The CNN has good effects on end-to-end image segmentation, often used for cell segmentation. However, because the signal transmission of CNN only occurs with the previous layer, the RNN is proposed then. The structure diagram of the RNN is shown in Figure 2, where the nodes between the hidden layers are interconnected. The specific single-node recurrent structure is shown in Figure 3.

2.3. The Structure of the DC-U-Net Model. The DC-U-Net model includes a contraction path and an expansion path. The contraction path is to collect the characteristics of the data, with the expansion path for accurate positioning, and the two are symmetrical to each other. The contraction path performs downsampling through maximum pooling of 2×2 , and the number of feature channels is doubled for each downsampling, with the resolution halved. In the expansion path, the upsampling is performed on the feature map, and a corresponding mirror map of the contraction path is generated, with information between the high and low layers fused to maximize

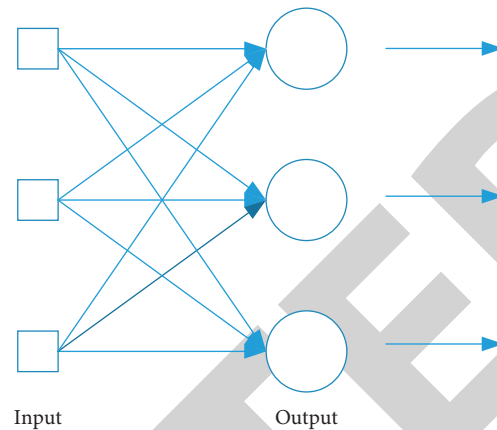


FIGURE 1: The working process of a neuron.

the retention of the feature information in the sampling process. Then, the model fuses image features together and convolves the features after upsampling and mirror mapping. As a result, the image resolution is doubled, and the feature channel is halved. Finally, the feature vector is mapped to the output layer of the network to obtain the output feature map.

The input image resolution is set to 256×256 , and the convolution block contains a DC and the activation function. The size of the convolution kernel in the convolution layer is 3×3 , with the hyperparameter dilation interval introduced to measure the dilation size, and the activation function is the ReLu function. In the contraction path, the maximum pooling of 2×2 is used for downsampling. Each time after the downsampling, the image size is halved, with the number of feature channels doubled. After three convolutional blocks, a 1×1 convolutional layer is used to fuse multichannel features. In the expansion path, a 3×3 convolution structure is adopted and the upsampling is performed, during which the image resolution is doubled and the number of feature channels is halved. Then, the mirror mapping is used to achieve information fusion between the high layer and the low layer. A 1×1 convolutional layer is added to the model to fuse multichannel information and increase nonlinearity. The activation function of the output layer is the sigmoid function. Finally, a segmentation map of 256×256 is output.

2.4. The Evaluation Function of the DC-U-Net Model. The activation function endows the convolutional layer with the nonlinear expression ability missing in the operation. It is also a nonlinear function connecting the upper and lower layers, aiming to deal with more complex problems. Normally, the sigmoid function is used for classification output, and the ReLu function is selected to extract the internal features. The ReLu function is a modified linear unit with simple calculation process, fast calculation speed, and fast convergence speed. At the same time, it can effectively avoid gradient problems, which are superior to the sigmoid function.

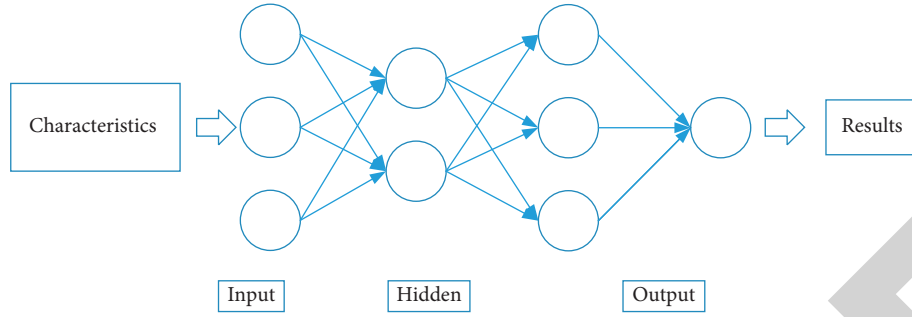


FIGURE 2: The schematic diagram of RNN structure.

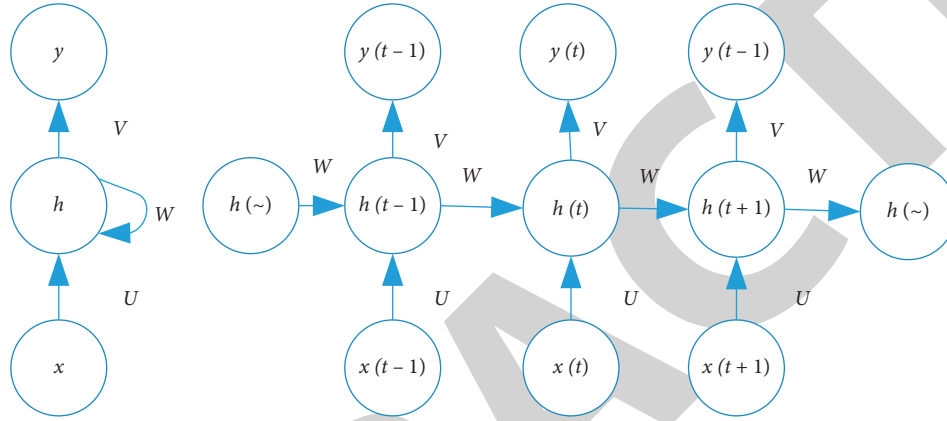


FIGURE 3: The schematic diagram of hidden layer structure.

The sigmoid function is expressed as follows:

$$S = \frac{1}{1 + e^{-z}} = \frac{1}{1 + e^{-(wx+b)}} \quad (1)$$

The ReLu function is expressed as follows:

$$R(z) = \max(0, z),$$

$$R'(z) = \begin{cases} 0 & z < 0 \\ 1 & z > 0 \end{cases} \quad (2)$$

The loss function is a function used to express the degree of deviation. A smaller loss function indicates a better performance of the model and the stronger robustness. A reasonable choice of loss function can train model parameters and optimize the model. The commonly used loss function is the cross-entropy loss function, expressed as follows:

$$C = -\frac{1}{n} \sum [y \log(f(I)) + (1 - y) \log(1 - f(I))]. \quad (3)$$

The Dice coefficient is a function that measures the similarity of sets, used to evaluate the overlap degree between two sets of samples, expressed as follows:

$$D = \frac{2|A \cap B|}{|A| + |B|} \quad (4)$$

where A and B represent the image mask pixels and the pixel matrix of the output predicted image. A Dice coefficient increasingly close to 1 indicates higher similarity between the predicted value and the true value.

2.5. The Image Segmentation by the DC-U-Net Model. The segmentation process of the DC-U-Net model is shown in Figure 4. First, the energy/spectral CT image of the patient was input, whose size was adjusted to 126 * 126 after preprocessing. 36 patients with the spinal metastasis from lung cancer were selected as the research subjects, with 5 energy/spectral CT images taken from each. A total of 180 images were randomly divided into the training set (135 photos) and validation set (45 photos) at a ratio of 3 : 1. Subsequently, the DC-U-Net model was trained by the training and verified with the validation set. Finally, the output image was compared with the original image.

2.6. Data Acquisition and Image Processing. The focus with the largest area was selected first for analysis, with the largest-layer whole tumor area method adopted to select the largest layer of the focus. A circular ROI of an appropriate size was put in the center of the lesion, with the focus surrounded as much as possible, away from bone fragments, obvious calcification areas, and the necrotic zone. Data measurement and analysis: the CT values of each ROI under 40–140 keV were recorded to draw the energy spectral curve of the focus, and the slope of the curve was calculated.

The CT value and SD value of the selected focus were recorded, respectively, as well as the average CT value and SD value of two background areas, which were taken as the CT value and SD value of the background area. With the SD value of the surface fat tissue taken as the noise intensity, the

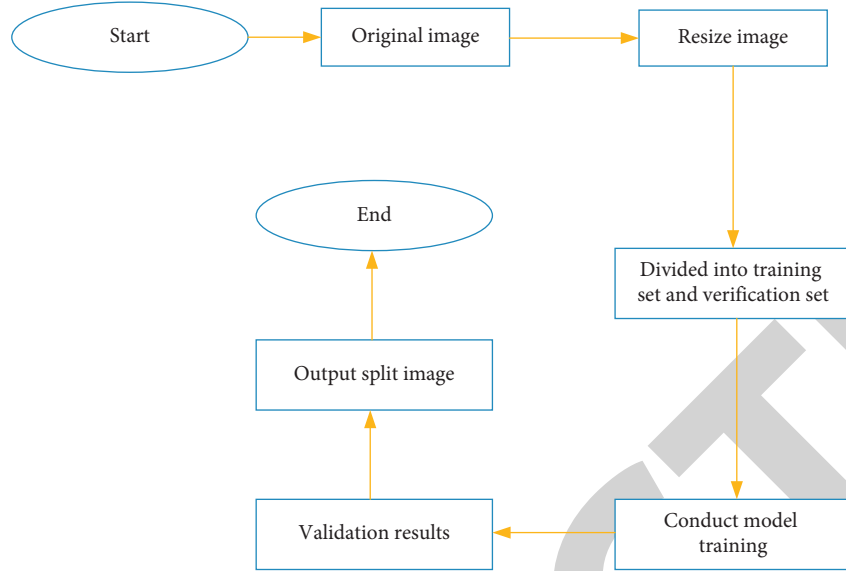


FIGURE 4: The segmentation process of the DC-U-Net model.

SNR value and the CNR value (between the focus and the vertebral body) were calculated:

$$\text{SNR} = \frac{X_{\text{focus}}}{SD_{\text{fat}}},$$

$$\text{CNR} = \frac{(X_{\text{focus}} - X_{\text{background}})}{SD_{\text{background}}},$$
(5)

where X represents the measured CT value.

2.7. Statistics. The data were processed by SPSS 21.0. The Shapiro–Wilk test was performed to verify whether the CT value and the curve slope satisfied the normality distribution, and the test standard was defined as $\alpha=0.1$. The quantitative data were expressed as a median, and Mann–Whitney U test was used for difference comparison. $P < 0.05$ was set as the threshold for significance.

3. Results

3.1. The Learning Rate Analysis. As shown in Figure 5, as the number of training increased, the learning rate gradually declined. When the number of training reached 24, the learning rate was almost close to zero. The total number of training was 50, while the learning rate started to approach 0 at 20 times.

The DC-U-Net model showed lower loss function and slightly higher Dice coefficient versus the CNN, no matter in the validation set or the training set. The validation set showed higher loss function versus the training set, with a notable difference. However, the difference in Dice coefficients between the two was not notable ($P > 0.05$) (Table 1).

3.2. Segmentation Results of the DC-U-Net Model. The segmentation algorithms for lung CT mainly include the threshold-based method, the boundary-based method,

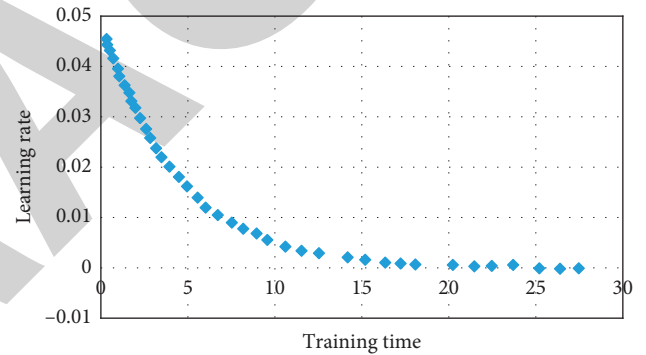


FIGURE 5: Exponential relationship between the learning rate and training times.

TABLE 1: Comparison of experimental results.

	Data	CNN	DC-U-Net
Loss	Training	0.0527	0.0464
	Validation	0.0704	0.0701
Dice	Training	0.9512	0.9621
	Validation	0.9431	0.9513

and the specific theory-based method. The lung is filled with a lot of air, and it manifested as a black area in the CT image. However, it is difficult to identify the boundaries of the target area in CT images, and blood vessels and small cavities around the lung parenchyma are always omitted. The DC-U-Net model proposed in this study was used to segment the energy/spectral CT image. Figure 6 shows the image before segmentation, and Figure 7 shows the image after segmentation. Although the DC-U-Net model segmented the lung out of the image, the segmentation margin was affected by blood vessels. Enlarging the training dataset can reduce the error, but at the same time, increase the training time.

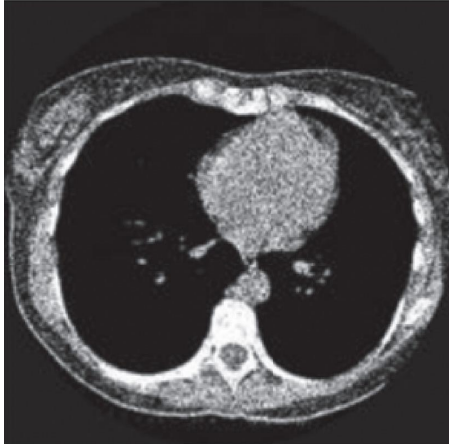


FIGURE 6: The energy/spectral CT image before segmentation.



FIGURE 7: The energy/spectral CT image after segmentation.

3.3. *The CT Values of Bone Metastasis from Lung Cancer under Different Energy Levels.* As shown in Figure 8, under 90–140 keV, the CT value corresponding to bone metastases from lung cancer and the slope of the curve relative to myeloma showed a downward trend.

As shown in Figure 9, under 40–55 keV, there were notable differences in rank sum test results of the myeloma and the lung cancer, with $P < 0.001$. Under 60–75 keV, there were notable differences in rank sum test results between the two, with $P < 0.01$. Under 80–90 keV, there were notable differences in rank sum test results between the two, with $P < 0.05$. Under 90–140 keV, there were notable differences in rank sum test results between the two, with $P > 0.05$.

3.4. *The SNR and CNR Values under Different Energy Levels.* As shown in Table 2, for a monoenergetic CT image, under 40 keV and 60 keV, the SNR and CNR values were higher than those under 140 kVp ($P < 0.05$); the SNR and CNR values under 60 keV were higher than those under 40 keV ($P < 0.05$); and the CNR value under 80 keV was higher than that under 140 kVp ($P < 0.05$).

As shown in Table 3, under 60 keV, the focus detection rate was the highest, notably higher than that under 140 kVp

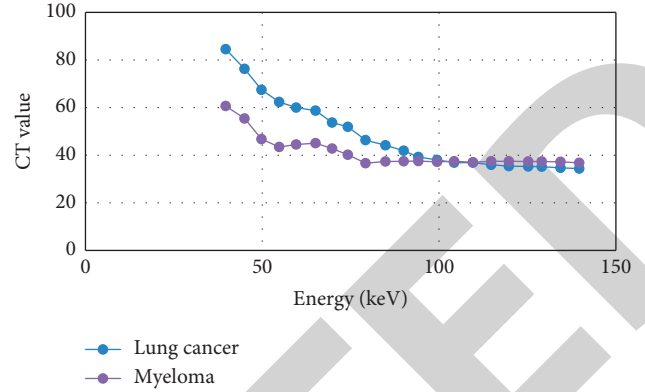


FIGURE 8: CT values of patients with myeloma and lung cancer at different energy levels.

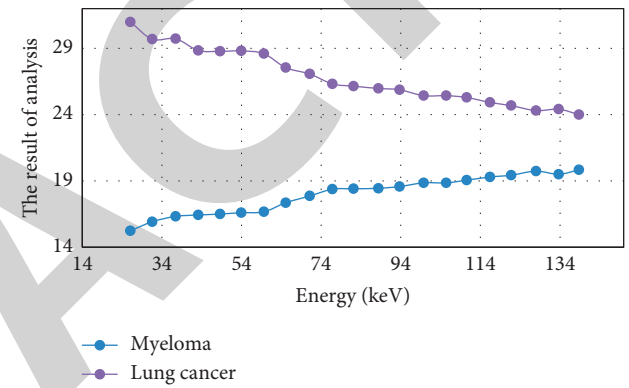


FIGURE 9: Comparison of rank sum test results between myeloma patients and lung cancer patients.

TABLE 2: The SNR and CNR values under different energy levels.

The energy level	Number of foci	SNR	CNR
140 kVp	88	48.12 ± 20.13	7.38 ± 3.46
40 keV	88	49.33 ± 19.67	7.26 ± 3.63
60 keV	88	65.02 ± 24.86	7.67 ± 3.85
80 keV	88	47.28 ± 17.01	7.53 ± 3.68
100 keV	88	38.96 ± 14.17	7.14 ± 3.36
120 keV	88	36.37 ± 12.86	6.93 ± 3.25
140 keV	88	34.73 ± 12.25	6.77 ± 3.21

($P < 0.05$). There was no notable difference in detection rates between the professional doctor and the deep learning algorithm.

4. Discussion

The bone metastasis from lung cancer is common, especially from small cell lung cancer and poorly differentiated nonsmall cell lung cancer. The incidence is about 30%, mostly in the spine, ribs, and femur. The early clinical symptoms of lung cancer bone metastasis are not obvious. When the pain appears, it is generally in the advanced stage. Bone metastases from lung cancer are mostly osteolytic, and sometimes pathological fractures and hypercalcemia occur [10, 11]. Lv et al. [12] proposed a low-dose CT detection method for lung nodule based on a three-

TABLE 3: The detection rates by different methods.

The energy level	The professional doctor			The deep learning algorithm		
	Detected	In total	The detection rate (%)	Detected	In total	The detection rate (%)
140 kVp	101	156	64.74	103	156	66.03
60 keV	121	156	77.56	127	156	81.41

dimensional CNN, and the detection accuracy was significantly improved. Zuo et al. [13] proposed a method to classify lung nodules using a three-dimensional CNN model. The sensitivity was 0.619, indicating good accuracy. Isotope scans are often used in clinical examinations, which can quickly show bone metastases throughout the body. Although the sensitivity is high, the specificity is low. Energy/spectral CT can show the local condition of bone metastases, with good specificity and positioning [14]. Energy/spectral CT imaging takes advantage of the difference in absorption of X-rays by substances under different energy levels to provide more information than conventional CT and improve image quality. Secondly, it effectively removes ray hardening artifacts, reduces radiation dose, and is suitable for qualitative and quantitative diagnosis of small foci. The K-edge imaging is adopted to reduce the dose of radiation and contrast agent, with soft tissue contrast improved by virtue of multi-energy spectrum characteristics. As a result, the tissue contrast with similar absorption coefficients of ray is enhanced, as well as the soft tissue contrast in lower energy regions. DC is convolution with intervals that can expand the field of view. The DC-U-Net model shows a higher information extraction ability without changing the image parameters [15].

This study focused on the detection rate of spinal metastases from lung cancer by energy/spectral CT processed by deep learning. The DC-U-Net model was used to segment the energy/spectral CT images of patients with spinal metastases from lung cancer. Then, energy/spectrum CT images at different energy levels were collected. The comparison of SNR and CNR found that the DC-U-Net model demonstrates better segmentation effects than CNN, and the lung contour was clearly segmented by the DC-U-Net model. It was also found in the study that the learning rate of the DC-U-Net model decreased exponentially as the number of training increased [16], and it can effectively segment the lung out of the energy/spectral CT image. Under 40 keV–90 keV, the CT value and the rank sum test result decreased with the increase of energy, which can clearly distinguish bone metastasis from lung cancer and myeloma. The SNR and CNR values under 60 keV were higher than those under 140 kVp ($P < 0.05$). Under 140 kVp and 40 keV, there was no notable difference in the detection rates by the deep learning algorithm (66.03%, 81.41%) and the professional doctor (64.74%, 77.56%) ($P > 0.05$), indicating that the deep learning algorithm demonstrates superb capabilities in the focus detection.

5. Conclusion

In the study, it was noted that the DC-U-Net model had lower loss function and higher Dice coefficient versus the CNN, which demonstrated better segmentation effects, with

the lung effectively segmented out of the CT image. What's more, the learning rate of DC-U-Net model was inversely proportional to the number of training times. The CT value of the bone metastasis focus from lung cancer was decreased with the energy level, and the rank sum test result was inversely proportional to the energy level. Under 60 keV, the image had the highest SNR and CNR values. Furthermore, the detection rate by the deep learning algorithm was close to that by the professional doctor. However, some limitations should be noted in the study. The sample size is relatively small, and the research is limited to the plain scan. A more comprehensive study on the diagnostic value of energy/spectral CT for bone metastasis from lung cancer may be necessary to strengthen the findings. The study provides a theoretical basis for the diagnosis of bone metastasis from lung cancer by the energy/spectral CT image.

Data Availability

No data were used to support this study.

Conflicts of Interest

The authors declare that they have no conflicts of interest.

Acknowledgments

This work was supported by the Key Science and Technology Research Plan of Hebei Province (No. 20150744).

References

- [1] H. H. Popper, "Progression and metastasis of lung cancer," *Cancer and Metastasis Reviews*, vol. 35, no. 1, pp. 75–91, 2016.
- [2] G. T. Silva, L. M. Silva, A. Bergmann, and L. Thuler, "Bone metastases and skeletal-related events: incidence and prognosis according to histological subtype of lung cancer," *Future Oncology*, vol. 15, no. 5, pp. 485–494, 2019.
- [3] B. La Combe, S. Gaillard, S. Bennis et al., "Prise en charge des métastases rachidiennes de cancer bronchopulmonaire [Management of spinal metastases of lung cancer]," *Revue des Maladies Respiratoires*, vol. 30, no. 6, pp. 480–489, 2013.
- [4] Q. Xu, M. Li, M. Li et al., "Energy spectrum CT image detection based dimensionality reduction with phase congruency," *Journal of Medical Systems*, vol. 42, no. 3, Article ID 49, 2018.
- [5] G. Wang, D. Zhao, Z. Ling et al., "Evaluation of the best single-energy scanning in energy spectrum CT in lower extremity arteriography," *Experimental and therapeutic medicine*, vol. 18, no. 2, pp. 1433–1439, 2019.
- [6] C. H. McCollough, S. Leng, L. Yu et al., "Dual- and multi-energy CT: principles, technical approaches, and clinical applications," *Radiology*, vol. 276, no. 3, pp. 637–653, 2015.

- [7] J. H. Lee, D. H. Kim, S. N. Jeong, and S. Choi, "Detection and diagnosis of dental caries using a deep learning-based convolutional neural network algorithm," *Journal of Dentistry*, vol. 77, pp. 106–111, 2018.
- [8] S. Afshar, S. Afshar, E. Warden et al., "Application of artificial neural network in miRNA biomarker selection and precise diagnosis of colorectal cancer," *Iranian Biomedical Journal*, vol. 23, no. 3, pp. 175–183, 2019.
- [9] P. Bándi, M. Balkenhol, B. van Ginneken et al., "Resolution-agnostic tissue segmentation in whole-slide histopathology images with convolutional neural networks," *PeerJ*, vol. 7, Article ID e8242, 2019.
- [10] S. L. Wood, M. Pernemalm, P. A. Crosbie et al., "The role of the tumor-microenvironment in lung cancer-metastasis and its relationship to potential therapeutic targets," *Cancer Treatment Reviews*, vol. 40, no. 4, pp. 558–566, 2014.
- [11] C. Gerecke, S. Fuhrmann, S. Striffler et al., "The diagnosis and treatment of multiple myeloma," *Deutsches Arzteblatt international*, vol. 113, no. 27-28, pp. 470–476, 2016.
- [12] X. Lv, L. Wu, Y. Gu et al., "Detection of low dose CT pulmonary nodules based on 3D convolution neural network," *Guangxue Jingmi Gongcheng/Optics and Precision Engineering*, vol. 26, no. 5, pp. 1211–1218, 2018.
- [13] W. Zuo, F. Zhou, Y. He et al., "Automatic classification of lung nodule candidates based on a novel 3D convolution network and knowledge transferred from a 2D network," *Medical Physics*, vol. 46, no. 12, pp. 5499–5513, 2019.
- [14] D. Wang, Y. Luo, D. Shen et al., "Clinical features and treatment of patients with lung adenocarcinoma with bone marrow metastasis," *Tumori*, vol. 105, no. 5, pp. 388–393, 2019.
- [15] X. P. Wang, B. Wang, P. Hou et al., "Screening and comparison of polychromatic and monochromatic image reconstruction of abdominal arterial energy spectrum CT," *Journal of Biological Regulators and Homeostatic Agents*, vol. 31, no. 1, pp. 189–194, 2017.
- [16] Z. Wang, Y. Ni, Y. Zhang et al., "Laparoscopic varicocele-tomy: virtual reality training and learning curve," *Journal of the Society of Laparoendoscopic Surgeons: Journal of the Society of Laparoendoscopic Surgeons*, vol. 18, no. 3, Article ID e2014.00258, 2014.